JOURNAL OF HARD TISSUE BIOLOGY
ISSN / eISSN 1341-7649
Publisher JOURNAL HARD TISSUE BIOLOGY,
JAPANESE RED CROSS SOCIETY, 3- 24- 20,
NISHIAZABU, MINATO KU,
JAPAN, TOKYO, 106-0031,
Volume 26-Issue 1-(2026)
DOI:https://doi-004.org/6812/17755446327718

Ferroptosis in Precancerous Lesions of Gastric Cancer Induced by Serum Containing *Isodon amethystoides*

Xing Zhang[1], Zhe Zhang[1] , Chungen Yan[1,*]

[1]*The Department of Gastroenterology, Shaoxing University Affiliated Hospital, Shaoxing, Zhejiang, 3 12000, China*
*Corresponding authors:Chungen Yan; *Email addresses*: 2010001229@usx.edu.cn (Chungen Yan)
Running title：Ferroptosis in Precancerous Lesions Induced by *Isodon amethystoides*

Abstract:

Background: Targeting precancerous lesions of gastric cancer (PLGC), defined as chronic atrophic gastritis accompanied by intestinal metaplasia and atypical hyperplasia, represents a promising strategy for early gastric cancer prevention. Weifuchun, a traditional Chinese medicine formulation, has been reported to ameliorate atrophic gastritis and intestinal metaplasia. *Isodon amethystoides* (Xiangcaicha), a primary component of Weifuchun, exhibits antitumor activity, modulates reactive oxygen species (ROS) levels, and promotes ferroptosis in cancer cells. Our previous investigations revealed differential expression of *Bmal1*, a gene closely associated with ferroptosis, across PLGC, gastric cancer tissues, and adjacent non-tumorous tissues.

Methods: We established an in vitro PLGC model by inducing malignant transformation in GES-1 human gastric epithelial cells using N-methyl-N'-nitro-N-nitrosoguanidine (MNNG), resulting in precancerous lesion cells (designated MC cells). We subsequently evaluated the effects of treatment with *Isodon amethystoides*-containing serum and we also predicted and primarily verified the targets of *Isodon amethystoides* based on network pharmacology analysis.

Results: Our findings demonstrate that MC cells treated with *Isodon amethystoides* exhibited characteristic mitochondrial morphological alterations consistent with ferroptosis, downregulation of glutathione peroxidase 4 (GPX4) expression, and significant elevations in intracellular iron ion concentration, malondialdehyde (MDA) levels, and ROS production. Besides, we revealed roles of PI3K/Akt signaling pathway and p53 in the ferroptosis.

Discussion: These findings suggest that Isodon amethystoides inhibits MC cells proliferation and promotes ferr.optosis by inhibiting PI3K/Akt signaling pathway and regulating p53.

Conclusion: These results collectively indicate that *Isodon amethystoides* impedes PLGC progression by promoting ferroptosis and the involvement of PI3K/Akt pathway and p53 in the ferroptosis.

Keywords: Precancerous Lesions of Gastric Cancer, Ferroptosis, *Isodon amethystoides*, Traditional Chinese Medicine, glutathione peroxidase 4, AKT, p53.

1. INTRODUCTION

Gastric cancer (GC) remains a major global health burden, ranking as the fifth most common malignancy in terms of incidence and mortality worldwide [1]. Early-stage GC detection rates remain disappointingly low, approximately 4.9%, with the majority of patients diagnosed at locally advanced or metastatic stages, contributing to an overall 5-year survival rate of only 30–35% [2]. Gastric carcinogenesis follows a well-defined pathological sequence: superficial gastritis progresses to atrophy, followed by intestinal metaplasia, dysplasia, and ultimately invasive carcinoma [3]. Gastric mucosal atrophy and intestinal metaplasia are considered precancerous conditions, while dysplasia is recognized as a precancerous lesion (PLGC). Consequently, interventions targeting PLGC represent a crucial strategic approach for GC prevention. Further elucidation of the mechanisms underlying malignant transformation in PLGC is essential for halting GC development. Currently, no universally effective pharmacological agents specifically target PLGC; management primarily focuses on eliminating causative factors, such as *Helicobacter pylori* eradication, anti-bile reflux therapy, and endoscopic interventions [4, 5]. Therefore, identifying effective therapeutics capable of arresting PLGC carcinogenesis, and potentially inducing regression, represents an urgent unmet clinical need.

Previous studies have indicated that Weifuchun, a traditional Chinese medicine formulation, can ameliorate gastric mucosal atrophy and intestinal metaplasia. Clinical gastroscopic and histopathological evaluations have demonstrated that Weifuchun improves pathological features in PLGC patients, particularly in cases of atrophy or intestinal metaplasia [6]. *Isodon amethystoides* (Xiangcaicha), a major active component of Weifuchun, possesses documented antitumor properties. Reports indicate that glaucocalyxin A, an active constituent of *Isodon amethystoides*, activates the ROS-mediated ATF4/CHOP/CHAC1 signaling axis in oral squamous cell carcinoma, thereby modulating cancer cell activity [7]. Similarly, glaucocalyxin B enhances cisplatin sensitivity in ovarian cancer cells by increasing intracellular ROS levels [8]. Our prior research identified differential expression of *Bmal1*, a gene strongly correlated with ferroptosis, among GC tissues, precancerous tissues, and chronic non-atrophic gastritis tissues, suggesting potential dysregulation of ferroptosis-related genes in PLGC.

Ferroptosis is a unique form of regulated cell death, distinct from apoptosis and autophagy, characterized by iron-dependent accumulation of lipid peroxides. Its core mechanism involves glutathione (GSH) depletion leading to inactivation of glutathione peroxidase 4 (GPX4), resulting in uncontrolled ROS accumulation during lipid peroxidation [9]. This process disrupts cellular integrity, compromises membrane fluidity and permeability, and ultimately culminates in cell death [10]. Based on these observations, we hypothesized that *Isodon amethystoides* might induce ferroptosis in PLGC. To test this, we prepared *Isodon amethystoides*-containing serum and investigated its effects on ferroptosis-

associated markers in MC cells.

2. MATERIALS AND METHODS

2.1 Cell Culture

Human immortalized gastric epithelial GES-1 cells were purchased from the Institute of Biochemistry and Cell Biology, Chinese Academy of Sciences (Shanghai, China). The cells were maintained in Dulbecco's Modified Eagle Medium (Wuhan Pricella Biotechnology Co, Ltd, Chin a) supplemented with 10% fetal bovine serum at 37°C in a humidified 5% CO_2 atmosphere. Mycopl asma contamination was excluded using the GMyc-PCR Mycoplasma Test Kit (Wuhan Pricella Bi otechnology Co., Ltd, China). Cell line authentication was performed through short tandem repeat (STR) profiling analysis. To induce malignant transformation, GES-1 cells were treated with 20 μM MNNG (Sigma-Aldrich, St. Louis, MO, USA) for 24 hours in the dark. Following MNNG exposure, cells were cultured in standard RPMI 1640 medium. Initial cell death was observed, followed by the outgrowth of surviving, transformed cells (designated MC cells)[11-13].

2.2 Animals

Eight-week-old (SPF grade) Sprague-Dawley rats were purchased from Shanghai SLAC Laborato ry Animals Co., Ltd (NO. SCXK (Hu) 2022-0004) and maintained under specific pathogen-free (SPF) conditions at the animal facility of Institute of Animal Laboratory of China Jiliang University. Fifty-five rats were randomly allocated into four groups: vehicle control (physiological saline, n=10), low-dose *Isodon amethystoides* extract (40 g/kg, n=15), moderate-dose extract (60 g/kg, n=15), and high-dose extract (80 g/kg, n=15). The dosages of *Isodon amethystoides* extract were referenced from previous descriptions [14, 15]. The animal studies were reviewed and approved by the Ethics Committee of China Jiliang University (permit NO. 2025-40). All experiments were performed in accordance with the ARR IVE guidelines (https://arriveguidelines.org) and regulations, and all procedures for animal experiments followed the ethical standards.

2.3 Preparation of *Isodon amethystoides*-Containing Serum

Isodon amethystoides pieces were weighed, soaked in 10 volumes of distilled water overnight, and subsequently boiled for 2 hours. The decoction was filtered through gauze repeatedly, and the combined filtrate was concentrated. Absolute ethanol was added to achieve a final concentration of 70%. The mixture was stirred thoroughly, allowed to stand for 24 hours, filtered to remove precipitates, and concentrated to obtain an ethanol-free extract stored at 4°C.

For drug-containing serum preparation, the extract was dissolved in physiological saline. Rats received the solution via oral gavage (1 mL/100g body weight) twice daily for 7 consecutive days. One hour after the final administration, blood was collected aseptically from the abdominal aorta. Serum was separated by centrifugation (5000 rpm, 10 min, 4°C), filtered, and stored at -80°C.

2.4 LC-MS/MS Analysis

Chemical profiling was performed using a UHPLC system (Vanquish, Thermo Fisher Scientific) equipped with a Phenomenex Kinetex C18 column (2.1 mm × 100 mm, 2.6 μm) coupled to an Orbitrap Exploris 120 mass spectrometer (Thermo Fisher Scientific). Mobile phases consisted of 0.01% acetic acid in water (A) and a 1:1 (v/v) mixture of isopropanol and acetonitrile (B). The autosampler temperature was maintained at 4°C, with an injection volume of 2 μL. MS/MS spectra were acquired using Xcalibur software with ESI source parameters set as follows: sheath gas flow 50 Arb, auxiliary gas flow 15 Arb, capillary temperature 320°C, full MS resolution 60,000, MS/MS resolution 15,000, stepped NCE 20/30/40, and spray voltages of +3.8 kV (positive) or -3.4 kV (negative).

2.5 Cell Viability Measurement

MC cells were seeded at a density of 5,000 cells per well into a 96-well plate. Cells were treated with drugs at different concentrations the next day. After 48 h, 10 μL CCK8 reagent was added into medium and cells were incubated at 37°C for 1 h. The absorbance at 450 nm was measured by a microplate reader (Bio Tek, USA).

2.6 Transmission Electron Microscopy (TEM)

MC Cells (~10^7) were fixed in 2.5% glutaraldehyde at 4°C for 24 hours, washed with PBS, post-fixed in 1% osmium tetroxide for 2 hours, and processed through embedding, polymerization, and lead citrate staining. Mitochondrial ultrastructure was examined using TEM.

2.7 Western Blotting

MC Cells were lysed using T-PER Tissue Protein Extraction Reagent (Thermo Pierce) supplemented with Halt Protease and Phosphatase Inhibitor Cocktail (Thermo Pierce). Lysates were centrifuged (12,000 rpm, 10 min), separated by SDS-PAGE (12.5% gel), and transferred to PVDF membranes (0.2 μm; Merck Millipore). Membranes were blocked with 5% BSA in TBST and incubated with primary antibodies against N-cadherin (1:10,000; ab76011; Abcam), p-STAT3 (1:2,000; 9145; Cell Signaling Technology), β-actin (1:1,000; ab8226; Abcam), GAPDH (1:1,000; 2118S, Cell Signaling

Technology), GPX4 (1:1,000; ab125066; Abcam), p-AKT (1:1,1000; AP0637, ABclonal), AKT (1:1,1000; A22770, ABclonal), p-p53 (1:1,1000; AP1504, ABclonal) and p53 (1:1,1000; A19585, ABclonal). After washing, membranes were incubated with HRP-conjugated secondary antibodies, and signals were detected using chemiluminescence (ChemiDoc, Bio-Rad).

2.8 Measurements of Iron, Malondialdehyde (MDA), and ROS

Intracellular iron content was quantified using a Cell Total Iron Colorimetric Assay Kit (Elabscience). Cells (~10^6) were lysed, and supernatants were incubated with chromogenic solution. Absorbance was measured at 593 nm (SpectraMax M5/M5e, Molecular Devices). Iron concentrations were determined from a standard curve.

MDA levels were assessed using a Colorimetric Assay Kit (Elabscience). Cell pellets (~3×10^6 cells) were homogenized, mixed with working solution, heated at 100°C for 40 min, centrifuged, and supernatant absorbance was measured at 532 nm. MDA concentrations were calculated via standard curve.

ROS levels were determined fluorometrically using DCFH-DA (Elabscience). Cells were incubated with 10 μM DCFH-DA for 30 min at 37°C in the dark, washed, and fluorescence was measured (excitation 500 nm, emission 525 nm).

2.9 Network Pharmacology

The blood components detected in the serum were analyzed for their pharmacophoric properties on the ADMET-AI platform, and those that met the Lipinski's Rule of Five, oral bioavailability more than 30% and Quantitative Estimate of Drug-likeness more than 0.5 were selected. The selected drug components were predicted to correspond to the targets in the TCMSP, Chembl and STITCH databases. Among them, Chembl screened the targets with an 80% confidence level of "active" and "both" and a threshold greater than 6, while STITCH screened the targets with a score greater than 300. Using "gastric carcinoma" as the keyword, potential targets for gastric cancer were predicted in the GeneCard, OMIM and TTD databases respectively. The targets were selected based on a relevance score of >10. The protein-protein interaction (PPI) network analysis was established on the base of STRING database. All targets were queried the protein interaction relationships in the STRING database for Homo sapiens (human) and then we constructed the network interaction map of the target proteins. In the PPI network, the Degree value is a crucial topological parameter, representing the number of other nodes (proteins) that a given node (protein) is connected to in the network. Nodes with higher Degree values are typically regarded as "knots" or "centroids" in the network, and may play more critical roles in biological processes. Next, using the network python library, the Degree values of each node in the network

interaction graph are calculated and arranged from largest to smallest and we got the core target network interaction graph.

2.10 Statistical Analysis

Data are presented as mean ± SEM from three independent experiments. Comparisons between two groups used Student's t-test; multiple group comparisons employed one-way ANOVA followed by Tukey's post hoc test. Statistical significance was set at $P < 0.05$. Analyses were performed using GraphPad Prism 9.0.

3. RESULTS

3.1 Analysis Chemical Constituents in *Isodon amethystoides*-Containing Serum

LC-MS/MS analysis of rat serum following *Isodon amethystoides* administration identified numerous compounds. Representative total ion chromatograms (TIC) in positive and negative ion modes are shown in Fig. 1. Based on fold change, the top 10 peak-associated substances are highlighted. Preliminary identification using the OTCML database suggested 899 and 913 compounds in positive and negative ion modes, respectively, with phenols and terpenoids constituting major fractions.

3.2 Characterization of MC Cells

N-nitro compounds (NOC) as strong carcinogens are main risk factor for gastric cancer. MNNG, as one of the most active carcinogenic NOCs has been reported to be successfully used to induce human gastric mucosal epithelial cells into precancerous cell model [16]. It was shown that the cell morphology of MC cells was bigger and exhibited more unclear cell edges compared with normal GES-1 cells (Fig. 2A). Epithelial-mesenchymal transition (EMT) is involved in the development of GC. The expression of level of N-cadherin, the mesenchymal marker, was significantly increased after MNNG treatment (P <0.01, Fig. 2B and C), which was consistent with the progression of gastric carcinogenesis. Furthermore, STAT3 plays a crucial role in the development of EMT in tumor cells. It has been demonstrated that MNNG could upregulate the expression of STAT3 phosphorylation (p-STAT3). We then measured the effects of MNNG on p-STAT3 by western blot and results revealed that the upregulation of p-STAT3 expression (P <0.01, Fig. 2B and D), which was similar to the previous results.

3.3 *Isodon amethystoides* Promotes Ferroptosis in MC Cells

Given the association between PLGC and ferroptosis, we first measured the effect of drug-contained serum on the viability of MC cells. MC cells were cultured with concentrations of serum samples and

erastin (a known ferroptosis inducer) for 48 h and we found that *Isodon amethystoides* reduced the viability of MC cells in a dose-response manner, where high dosage reduced the survival of cells to approximately lower than half of the normal (Fig. 3A). Then, we investigated whether *Isodon amethystoides* exerts antitumor effects via ferroptosis induction. TEM revealed that MC cells treated with erastin or *Isodon amethystoides*-containing serum exhibited characteristic mitochondrial changes. In the control group, the mitochondria exhibited an intact structure, regular morphology, intact and well-defined membranes and a uniform matrix density. Following treatment with drugs, the mitochondria displayed condensation, deformation, increased membrane density, and a reduction in cristae. These ultrastructural alterations suggest that *Isodon amethystoides* disrupts mitochondrial function in MC cells and is associated with the induction of ferroptosis (Fig. 3B).

GPX4, a key ferroptosis regulator, was significantly downregulated following erastin and *Isodon amethystoides*-containing serum treatments ($P < 0.01$, Fig.3C). The moderate-dose group showed the most pronounced GPX4 reduction ($P < 0.01$ vs. low and high doses).

Ferroptosis also features iron accumulation and lethal lipid ROS. Iron content significantly increased in all *Isodon amethystoides* serum-treated groups versus control ($P < 0.005$, Fig. 3D), with the highest level in the high-dose group. In addition, MDA and ROS levels were markedly elevated in all treatment groups ($P < 0.01$ and < 0.005, respectively), with the high-dose group showing the highest increases, consistent with erastin effects (Fig. 3E and F). These data collectively indicate that *Isodon amethystoides* promotes ferroptosis in MC cells, potentially retarding PLGC progression.

3.4 The PI3K/AKT/ signaling pathway and p53 are involved in ferroptosis induced by *Isodon amethystoides* in MC cells

Qualified metabolites were imported to the TCMSP, Chembl and STITCH databases to obtain the metabolites targets, and we totally got 1,592 target proteins. Moreover, we acquired 2,518 target genes related to gastric carcinoma based on the GeneCards database. Taking the intersection with 1,592 drug targets, 321 genes were obtained as the potential targets for the anti-gastric cancer effect of *Isodon amethystoides* (Fig. 4A). In the GO enrichment analysis mainly participates in the process of cell proliferation and apoptosis (Fig. 4B), implying its role in suppressing cancer cell proliferation and promoting its apoptosis. In the KEGG pathway enrichment analysis, a total of 207 significant entries were detected ($P < 0.05$). Among them, PI3K/Akt signaling pathway was the one related to tumors in the top 10 entries (Fig. 4C). Furthermore, the core target network interaction graph based on the two target compilations, which were targets of metabolites and gastric carcinoma respectively, showed *AKT1* is the top one node, followed by *TP53* (Fig. 4D).

To further clarify the roles of the PI3K/Akt signaling pathway and p53 in the ferroptosis induced by *Isodon amethystoides*, western blot experiments were used to detect changes in the expression of phosphorylate AKT (p-AKT) and p53 (p-p53). The results revealed that *Isodon amethystoides* significantly reduced the expression of p-AKT while increasing the expression of p-p53 protein (Fig. 4E). These results demonstrated that *Isodon amethystoides* inhibited the phosphorylation of AKT and stimulated that of p53, which means that PI3K/Akt signaling pathway and p53 are involved in the ferroptosis.

4. DISCUSSION

The incidence rate of gastric cancer in China is 0.3314%, and the mortality rate is 0.2434%. Both the incidence rate and the mortality rate rank second in the world [17]. For advanced gastric cancer, the main treatment methods currently include chemotherapy, immunotherapy and targeted therapy [18]. However, these treatment methods have problems such as significant adverse reactions and poor patient tolerance. While surgical resection remains the primary curative option for GC [19], metastasis often limits survival. Exploring potential drug targets and developing new drug treatment strategies is not only of great significance for improving treatment efficacy, but also provides new ideas for addressing the challenges in the prevention and treatment of GC [20]. Many natural products have been confirmed effective to inhibit the progress of gastric cancer *in vitro* and *in vivo*. For example, baicalein can inhibit gastric cancer by regulating expression of Bcl-2 and Bax, and exhibits tumor inhibitory effects *in vivo* [21]. Tanshinone IIA has been reported that can inhibit GC stemness by elevating lipid peroxides and reducing GSH [22]. However, managing preneoplastic and early neoplastic lesions remains challenging.

Ferroptosis, characterized by iron-dependent lipid peroxide accumulation, represents a promising anticancer strategy. GPX4 is a central ferroptosis negative regulator. Its inhibitor RSL3 reduces viability and induces lipid radical accumulation in GC MGC-803 cells more than in normal GES-1 cells, suggesting heightened ferroptosis susceptibility in GC [23]. Iron accumulation catalyzes ROS-mediated cell death, countered by antioxidants like GSH and GPX4 [24]. GSH depletion also induces ferroptosis.

Given Weifuchun's efficacy in PLGC, we focused on its principal component, *Isodon amethystoides*. *Isodon amethystoides* and related species demonstrate antitumor activity against various cancer cell lines. Compounds like eriocalyxin B from *Isodon eriocalyx* inhibit triple-negative breast cancer metastasis [25]. Other isolates exhibit cytotoxicity against lung cancer A549 cells [26]. Jaridon 6, a diterpene from *Rabdosia rubescens* inhibits SIRT1 via the PI3K/Akt pathway, inducing autophagy and reducing GC drug resistance [27]. *Rabdosia rubescens* volatile oil downregulates key GC-related cytokines (TNF, IL1B, MMP9, PTGS2) and promotes apoptosis in GC cells [28]. However, effects of

Isodon amethystoides on PLGC has not been reported yet. In this study, we sought to its efficacy in PLGC treatment. To induce PLGC cell model, we applied MNNG to treat GES-1 cells, resulting in chemical carcinogenesis model MC cells. Then, we assessed the anti-precancerous lesions efficacy of *Isodon amethystoides* on MC cells. Our results demonstrate that *Isodon amethystoides*-containing serum inhibits cell viability and induces ferroptosis in MC cells by downregulating GPX4 and elevating iron, MDA, and ROS levels.

Considering the multi-target and multi-pathway treatment effects of the natural herbs, we explored the underlying mechanisms of *Isodon amethystoides* against PLGC by network pharmacology analysis. The results of network pharmacology research indicate that may *Isodon amethystoides* regulate processes such as cell proliferation, oxidative stress and cell apoptosis. And the involved signaling pathways include PI3K-Akt pathways, etc. Furthermore, the intersection analysis of drug targets and genes related to GC indicates that *Isodon amethystoides* may participate in ferroptosis by regulating p53, thereby exerting an anti-gastric cancer effect. We verified the results of network pharmacology analysis through in vitro experiments, western blotting analysis showed that significantly downregulated the expression of p-AKT and upregulated the that of p-p53, further indicating that it may induce ferroptosis by inhibiting PI3K/Akt signaling pathway and regulating p53. It has been found that p53 is a crucial modulator of ferroptosis and promotes ferroptosis by reducing the biosynthesis of GSH [29, 30]. These findings support further identification and purification of active *Isodon amethystoides* constituents for PLGC therapy. The precise mechanisms underlying *Isodon amethystoides*-induced ferroptosis warrant deeper investigation. Also, in order to verify the clinical feasibility of *Isodon amethystoides*, further *in vivo* experiments are needed to assess its efficacy and safety.

CONCLUSION

In conclusion, this study reveals that *Isodon amethystoides* promotes ferroptosis mainly via inhibiting PI3K/Akt signaling pathway and regulating p53 in malignantly transformed human gastric epithelial cells, highlighting its potential to suppress PLGC progression.

AUTHORS' CONTRIBUTIONS

Z. X and Y. C initiated the project, designed the experiments and wrote the manuscript; Z. Z conducted the experiments and assisted in manuscript preparation.

ETHICS APPROVAL AND CONSENT TO PARTIPATE

This study received ethical approval from the Ethics Committee of China Jiliang University (permit

NO. 2025-40).

HUMAN AND ANIMAL RIGHTS

All the experiments were in compliance with the National Institutes of Health Guide for the Care and Use of Laboratory Animals. This study adheres to internationally accepted standards for animal research, following the 3Rs principle. The ARRIVE guidelines were employed for reporting experiments involving live animals, promoting ethical research practices.

CONSENT FOR PUBLICATION

Not applicable.

AVAILABILITY OF DATA AND MATERIALS

All data generated or analyzed during this study are included in this published article.

FUNDING

This study was supported by Zhejiang Provincial Medical Association Clinical Medicine Research Project (2023ZYC-Z21).

CONFLICT OF INTEREST

The authors declare no conflicts of interest, financial or otherwise.

ACKNOLEDGEMENTS

None.

REFERENCES

[1] Bray, F., et al., *Global cancer statistics 2022: GLOBOCAN estimates of incidence and mortality worldwide for 36 cancers in 185 countries.* CA Cancer J Clin, 2024. **74**(3): p. 229-263.

[2] Rocken, C., *Predictive biomarkers in gastric cancer.* J Cancer Res Clin Oncol, 2023. **149**(1): p. 467-481.

[3] Jin, Z., W. Jiang, and L. Wang, *Biomarkers for gastric cancer: Progression in early diagnosis and prognosis (Review).* Oncol Lett, 2015. **9**(4): p. 1502-1508.

[4] Chen, Z., et al., *Progress and current status of molecule-targeted therapy and drug resistance*

in gastric cancer. Drugs Today (Barc), 2020. **56**(7): p. 469-482.

[5] Pimentel-Nunes, P., et al., *Management of epithelial precancerous conditions and lesions in the stomach (MAPS II): European Society of Gastrointestinal Endoscopy (ESGE), European Helicobacter and Microbiota Study Group (EHMSG), European Society of Pathology (ESP), and Sociedade Portuguesa de Endoscopia Digestiva (SPED) guideline update 2019.* Endoscopy, 2019. **51**(4): p. 365-388.

[6] Bian, Y., et al., *A correlational study of Weifuchun and its clinical effect on intestinal flora in precancerous lesions of gastric cancer.* Chin Med, 2021. **16**(1): p. 120.

[7] Wang, X., et al., *Glaucocalyxin A impairs tumor growth via amplification of the ATF4/CHOP/CHAC1 cascade in human oral squamous cell carcinoma.* J Ethnopharmacol, 2022. **290**: p. 115100.

[8] Zhang, T., et al., *Glaucocalyxin B Attenuates Ovarian Cancer Cell Growth and Cisplatin Resistance In Vitro via Activating Oxidative Stress.* Oxid Med Cell Longev, 2022. **2022**: p. 6324292.

[9] Linkermann, A., et al., *Synchronized renal tubular cell death involves ferroptosis.* Proc Natl Acad Sci U S A, 2014. **111**(47): p. 16836-41.

[10] Zheng, J. and M. Conrad, *The Metabolic Underpinnings of Ferroptosis.* Cell Metab, 2020. **32**(6): p. 920-937.

[11] Tong, Y., et al., *Zuojin Pill ameliorates chronic atrophic gastritis induced by MNNG through TGF-beta1/PI3K/Akt axis.* J Ethnopharmacol, 2021. **271**: p. 113893.

[12] Chu, Y.M., et al., *Fuzheng Nizeng Decoction regulated ferroptosis and endoplasmic reticulum stress in the treatment of gastric precancerous lesions: A mechanistic study based on metabolomics coupled with transcriptomics.* Front Pharmacol, 2022. **13**: p. 1066244.

[13] Wang, Y., et al., *Erianin, the main active ingredient of Dendrobium chrysotoxum Lindl, inhibits precancerous lesions of gastric cancer (PLGC) through suppression of the HRAS-PI3K-AKT signaling pathway as revealed by network pharmacology and in vitro experimental verification.* J Ethnopharmacol, 2021. **279**: p. 114399.

[14] Miao, M., et al., *Effects of the Rabdosia rubescens total flavonoids on focal cerebral ischemia reperfusion model in rats.* Saudi Pharm J, 2017. **25**(4): p. 607-614.

[15] Huang, G.D., et al., *[Effect of Isodon ternifolius-medicated serum on hepatic stellate cells based on TLR4/NF-κB/NLRP3 signaling pathway].* Zhongguo Zhong Yao Za Zhi, 2023. **48**(14): p. 3913-3921.

[16] Cai, Y., et al., *Study on the Mechanism of Sancao Tiaowei Decoction in the Treatment of MNNG-Induced Precancerous Lesions of Gastric Carcinoma Through Hedgehog Signaling*

Pathway. Front Oncol, 2022. **12**: p. 841553.

[17] Xia, C., et al., *Cancer statistics in China and United States, 2022: profiles, trends, and determinants.* Chin Med J (Engl), 2022. **135**(5): p. 584-590.

[18] Cao, W., et al., *Changing profiles of cancer burden worldwide and in China: a secondary analysis of the global cancer statistics 2020.* Chin Med J (Engl), 2021. **134**(7): p. 783-791.

[19] Tan, Z., *Recent Advances in the Surgical Treatment of Advanced Gastric Cancer: A Review.* Med Sci Monit, 2019. **25**: p. 3537-3541.

[20] Xing, P., et al., *Natural products in digestive tract tumors metabolism: Functional and application prospects.* Pharmacol Res, 2023. **191**: p. 106766.

[21] Mu, J., et al., *The Traditional Chinese Medicine Baicalein Potently Inhibits Gastric Cancer Cells.* J Cancer, 2016. **7**(4): p. 453-61.

[22] Ni, H., et al., *Tanshinone IIA inhibits gastric cancer cell stemness through inducing ferroptosis.* Environ Toxicol, 2022. **37**(2): p. 192-200.

[23] Zhao, L., et al., *Apatinib induced ferroptosis by lipid peroxidation in gastric cancer.* Gastric Cancer, 2021. **24**(3): p. 642-654.

[24] Fischbacher, A., C. von Sonntag, and T.C. Schmidt, *Hydroxyl radical yields in the Fenton process under various pH, ligand concentrations and hydrogen peroxide/Fe(II) ratios.* Chemosphere, 2017. **182**: p. 738-744.

[25] Gou, L., et al., *Natural product Eriocalyxin B suppressed triple negative breast cancer metastasis both in vitro and in vivo.* Biochem Pharmacol, 2023. **210**: p. 115491.

[26] Wei, W.J., et al., *Cytotoxic ent-Kaurane Diterpenoids from Rabdosia Rubescens.* Chem Biodivers, 2022. **19**(10): p. e202200497.

[27] Fu, L., et al., *Jaridon 6, a new diterpene from Rabdosia rubescens (Hemsl.) Hara, can display anti-gastric cancer resistance by inhibiting SIRT1 and inducing autophagy.* Phytother Res, 2021. **35**(10): p. 5720-5733.

[28] Hu, Y., et al., *Key Targets and Molecular Mechanisms of Active Volatile Components of Rabdosia rubescens in Gastric Cancer Cells.* Curr Comput Aided Drug Des, 2022. **18**(7): p. 493-505.

[29] Tarangelo, A., et al., *p53 Suppresses Metabolic Stress-Induced Ferroptosis in Cancer Cells.* Cell Rep, 2018. **22**(3): p. 569-575.

[30] Tajan, M., et al., *A Role for p53 in the Adaptation to Glutamine Starvation through the Expression of SLC1A3.* Cell Metab, 2018. **28**(5): p. 721-736.e6.

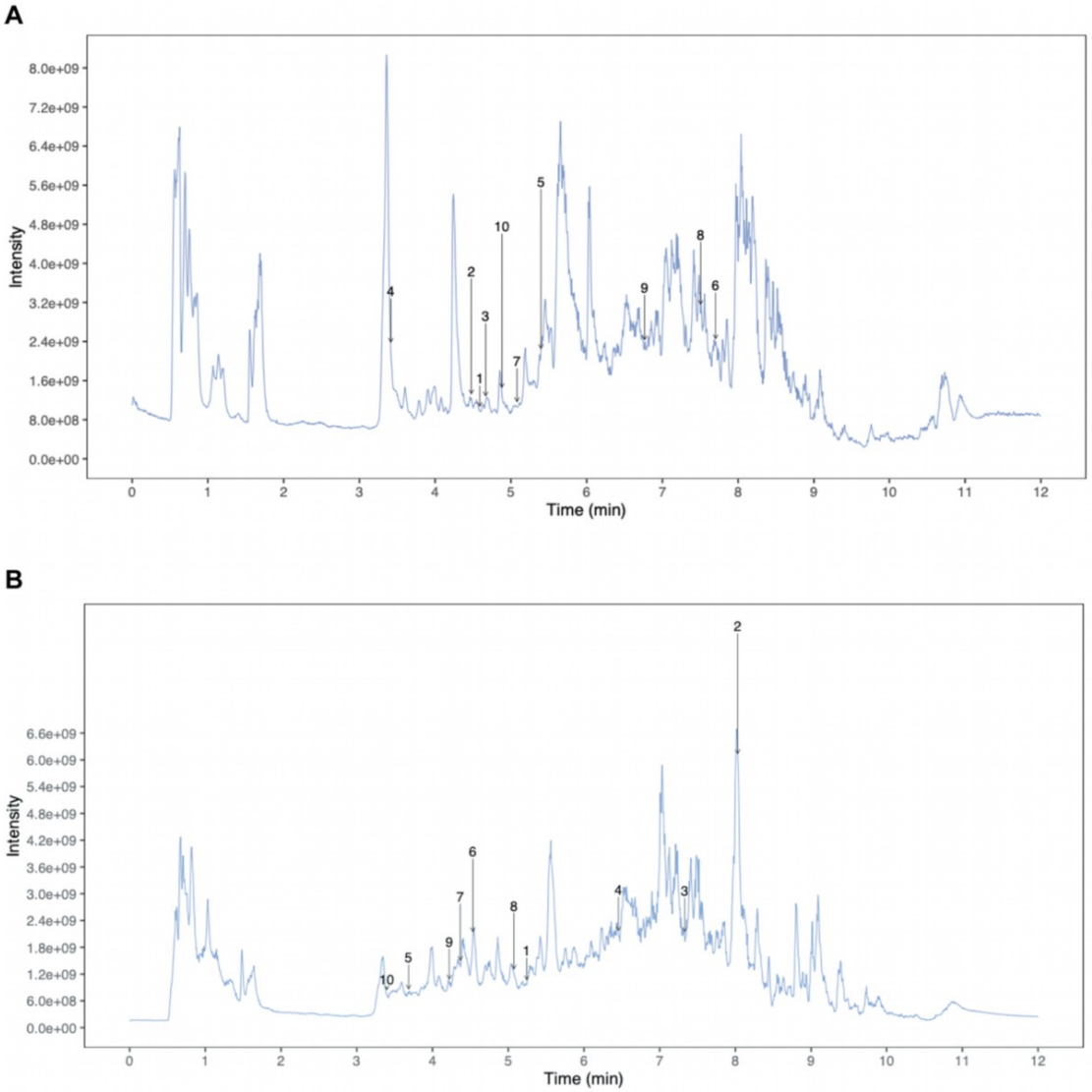

Fig. (1). Mass spectrum chromatograms of *Isodon amethystoides* containing serum. (**A**) Positive ion mode total ion chromatogram (TIC) of rat serum samples after isodon amethystoides intervention. (**B**) Negative ion mode total ion chromatogram (TIC) of rat serum samples after isodon amethystoides intervention.

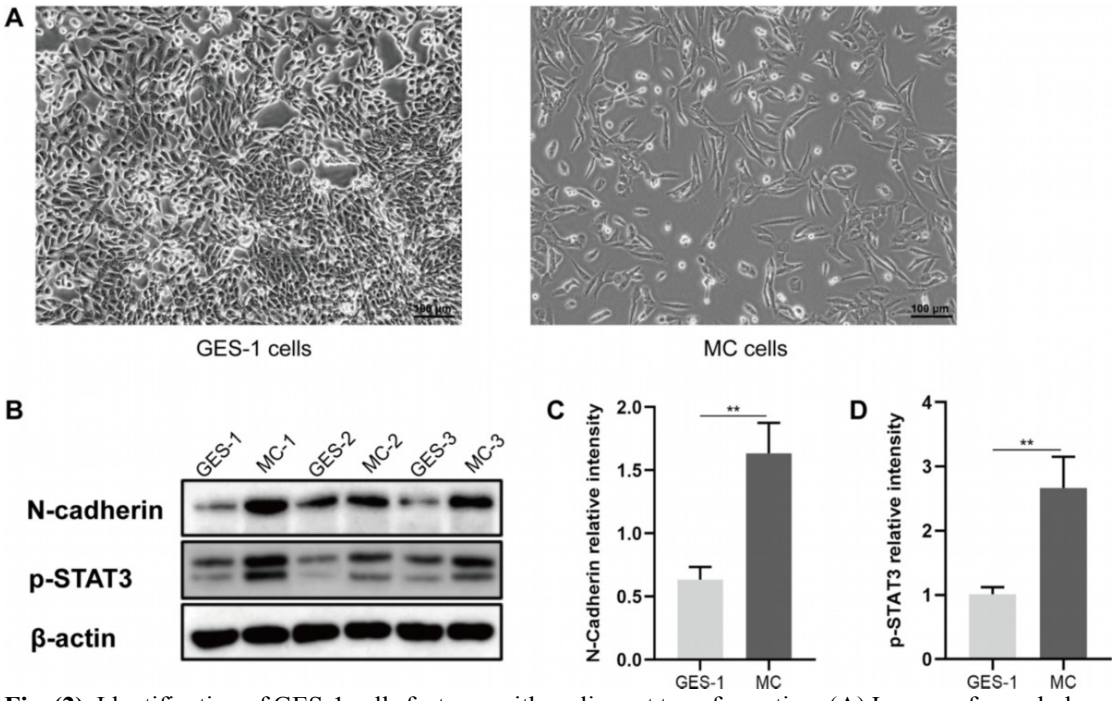

Fig. (2). Identification of GES-1 cells features with malignant transformation. (**A**) Images of morphology of normal GES-1 cells and malignant MC cells, scale bars, 100 μm. (**B**) Immunoblot images of N-cadherin and p-STAT3 expression in GES-1 and MC cells. (**C-D**) Quantitative densitometric analysis of N-cadherin (**C**) and p-STAT3 (**D**) in these cell lines. Data shown are means ± SEM of three independent experiments, normalized with respect to the β-actin expression. Statistical analysis was performed by unpaired *t* test. ***P*<0.01.

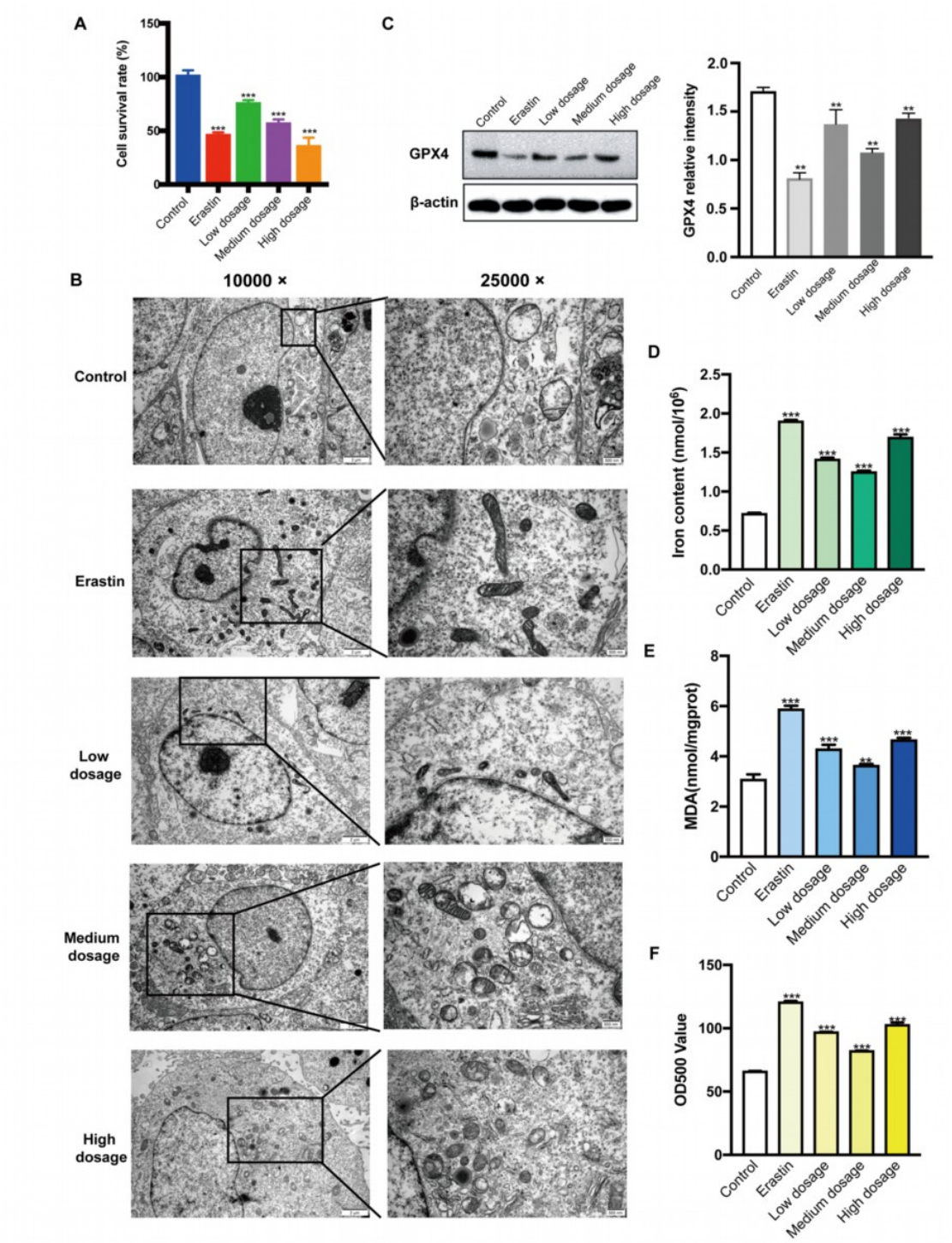

Fig. (3). Effects of ferroptosis promotion induced by *Isodon amethystoides* in MC cells. (**A**) The effect of drugs on the viability of MC cells using CCK8 kits. (**B**) Images of mitochondria in MC cells treated with different agents. (**C**) Expression of GPX4 in MC cells after drugs treatment. (**D-F**) The contents of iron ions (**D**), MDA (**E**) and ROS (**F**) in different treatment groups. Data shown are means ± SEM of three independent experiments. Statistical analysis was performed by one-way ANOVA followed by Dunnett's multiple comparison test. ***$P < 0.005$, **$P < 0.01$.

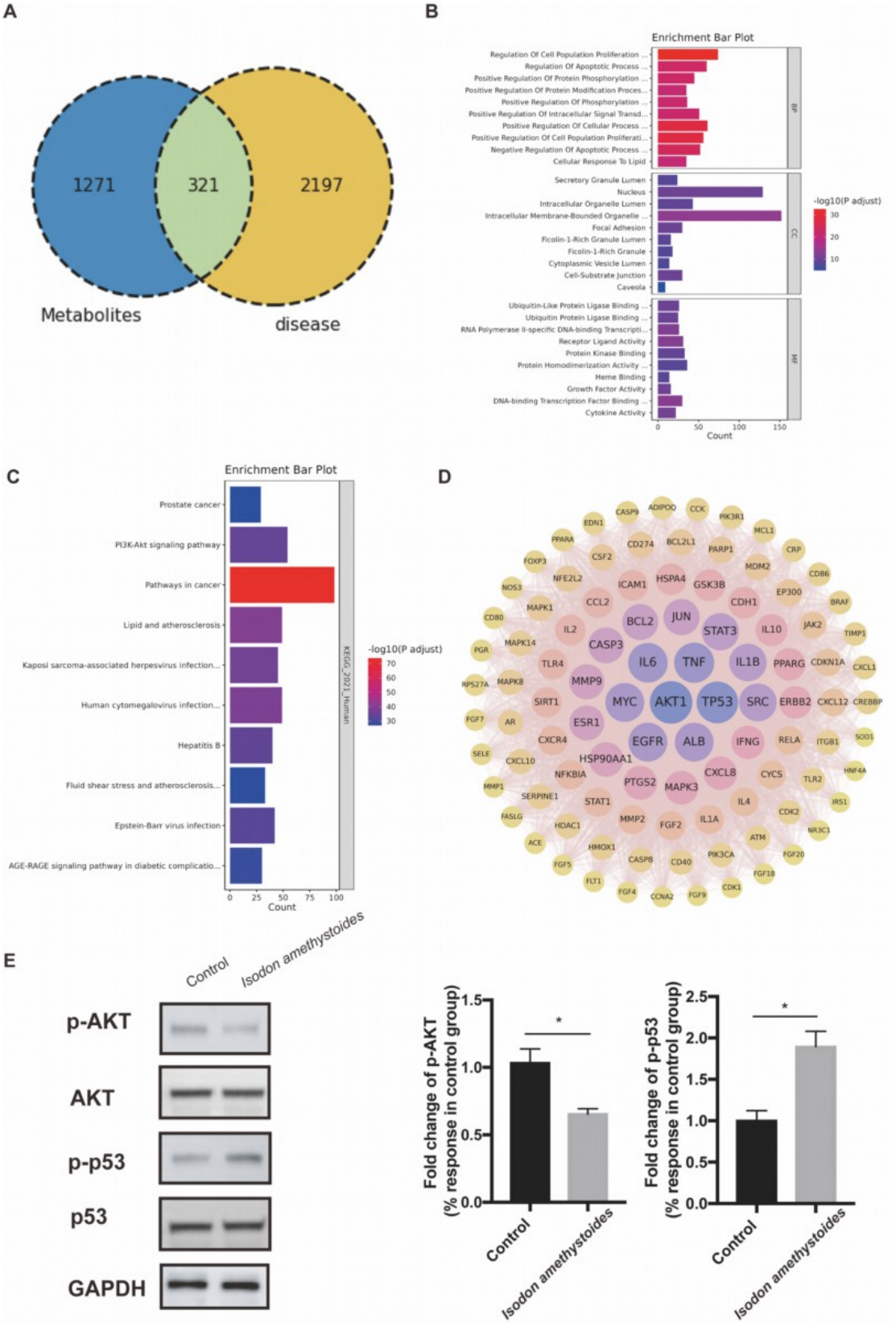

Fig. (4). The prediction and verification of the drug targets based on network pharmacology. (**A**) The Venn diagram of target genes of *Isodon amethystoides* and gastric carcinoma. (**B**) GO enrichment analysis. (**C**) KEGG pathway enrichment analysis. (**D**) PPI network analysis of intersecting targets between *Isodon amethystoides* and gastric carcinoma. (**E**) Effect of *Isodon amethystoides* on expression of PI3K/Akt pathway and p53. Data shown are means ± SEM of three independent experiments, normalized with respect to the GAPDH expression. Statistical analysis was performed by unpaired t test.

*$P < 0.05$.